The effect of nanocrystallized surface on the tribocorrosion behavior of 304L stainless steel

Fatma Ben Saada, Zied Antar, Khaled Elleuch, Pierre Ponthiaux, Nathalie Gey

The effect of nanocrystallized surface on the tribocorrosion behavior of 304L stainless steel

Fatma Ben Saada[a,*], Zied Antar[a], Khaled Elleuch[a], Pierre Ponthiaux[b], Nathalie Gey[c]

[a] Laboratoire de Génie des Matériaux et Environnement, LGME, Ecole Nationale d'Ingénieurs de Sfax, ENIS, Université de Sfax, B.P.X., 1173-3038 Sfax, Tunisia
[b] Laboratoire de Génie des Procédés et Matériaux, LGPM, Ecole Centrale Paris, F-92290 Chatenay-Malabry, France
[c] Laboratoire d'Etude des Microstructures et de Mécanique des Matériaux, LEM3, UMR CNRS 7239, Université de Lorraine, 54045 Metz Cedex 1, France

ARTICLE INFO

Keywords:
AISI 304L
Nanocrystallization
Tribocorrosion
Ferrite
Corrosion
Wear

ABSTRACT

A nanocrystallized surface layer of around 150 μm thickness was created on AISI 304L by nano-scale surface peening. Electron back scattered diffraction (EBSD) has revealed that the upper layer of the nanocrystallized surface was formed by nanosized ferrite grains. However, bottom layer was compounded from martensite and deformed austenite. Tribocorrosion behavior of the nanocrystallized surface against alumina was investigated in a mixture of olive pomace and tap water filtrate. Nanopeened 304L was more sensitive to tribocorrosion under intermittent sliding than continuous one due to depassivation/repassivation phenomena. Mechanical and corrosion wear components were quantified. Tribocorrosion mechanism was dominated by abrasion mechanical removal of the uncovered surface. The wear resistance of AISI 304L surface was markedly improved by treatment. That improvement could be explained by the higher hardness of nanocrystallized AISI 304L.

1. Introduction

Structure and properties of the surface affect effectively global behavior of materials. Surface microstructure as well as material properties may play an important role in failure control including cracking, wear and corrosion [1–3]. These kinds of degradation processes induce significant problems in olive oil industry, especially in the machinery. Particularly, the horizontal centrifuge was highly damaged by tribocorrosion due to the combined effect of mechanical wear and corrosion: In fact this equipment is composed by four metal raclettes and a cylindrical funnel made of AISI 304L to physically separate olive seeds from olive pulp [4].

The tribocorrosion behavior of AISI 304L/alumina contact was recently studied in sulphuric acid by Perret et al. [5]. A reciprocating tribometer was used with a reciprocating motion of 1 Hz frequency, 5 mm amplitude and 7 or 24 N as normal load. Authors have stated that a plastically deformed layer, characterized by a refined structure and the presence of structural defects, was developed. In our previous study [4], the tribocorrosion behavior of AISI 304L sliding against alumina was studied in a mixture of olive pomace and tap water filtrate. It was found that AISI 304L was sensitive to tribocorrosion especially under intermittent sliding. Moreover, mechanical removal wear loss was dominated by an abrasive wear mechanism. Therefore, improvement of AISI 304L surface properties could enhance the material behavior and consequently the service life of components.

Surface properties could be enhanced chemically [6–8], by adding a coating [9–11] or metallurgically [12–14]. The change of the surface chemistry could be realized by phosphate chemical conversion coatings [6], laser alloying [7] and nitriding [8]. Adding a coating could be obtained by laser cladding [9], physical vapour deposition (PVD) [10] or chemical vapour deposition (CVD) [11]. The change of the surface metallurgy could be developed by localized surface hardening (flame, induction, laser, and electron-beam hardening) [12], laser melting [13] or shot peening [14].

Different conventional mechanical surface treatments have been investigated, to improve surface behavior and to generate a nanocrystallized surface layer by severe plastic deformation methods such as surface mechanical attrition treatment [3], ultrasonic shot peening [15], ultrasonic cold forging technology [16] and severe shot peening [17]. These methods have improved fatigue properties, hardness, wear resistance and tensile strength [15]. The severe shot peening (SSP), an alternative method of the conventional shot peening, has received most of the attention of industrials because of its popularity and technological facility [17]. The SSP was developed using a conventional shot peening (eg. Air blast shot peening) by applying a combination of severe peening parameters. The parameters combination multiplies the kinetic energy compared to conventional shot peening and can produce a nanostructured surface layer [17–20]. Tadge et al. [21] have revealed

* Corresponding author.
E-mail address: fatma.ben.saada@hotmail.com (F.B. Saada).

Nomenclature

A_0	Sample area (cm^2)
A_{act}	Area of active material in the wear track
A_{repass}	Area of repassivated material in the wear track
Cdl	Double layer capacitance
COF	Coefficient of friction
EBSD	Electron Back Scattered Diffraction
BSE	Back Scattered Electron
EC	Electrical circuit
E_{corr}	Free corrosion potential (V/Ag-AgCl)
EIS	Electrochemical impedance measurements
E_{pit}	Pitting potential (V/Ag-AgCl)
E_{prot}	Protection potential (V/Ag-AgCl)
IPF	Inverse Pole Figure
K_c	Ratio of the specific material loss due to corrosion over the specific material loss due to mechanical wear in the wear track
K_m	Ratio of the specific material loss due to mechanical wear of the active material over the specific material loss due to mechanical wear of the repassivated material in the wear track
OCP	Open circuit potential
r_p	Specific polarization resistance ($\Omega\ cm^2$)
R_p	Polarization resistance (Ω)
R_s	Solution resistance (Ω)
SEM	Scanning electronic microscopy
SHE	Standard Hydrogen Electrode
SSP	Severe shot peening
t_{lat}	Latency time (s)
t_r	Rotation time (s)
t_{stop}	Stop time (s)
W_{tr}	Total wear (cm^3/cycle)
W^c_{act}	Material loss due to corrosion of active material in the wear track (cm^3/cycle)
W^m_{act}	Material loss due to mechanical wear of the active material in the wear track (cm^3/cycle)
W^c_{repass}	Material loss due to corrosion of repassivated material in the wear track (cm^3/cycle)
W^m_{repass}	Material loss due to the mechanical wear of repassivated material in the wear track (cm^3/cycle)
Z	Impedance
Z_{im}	Imaginary part of the impedance (Ω)
Z_{re}	Real part of the impedance (Ω)

that shot peened AISI 304 showed ultrafine austenite grains and martensitic transformation at severely deformed locations. The martensite phase and grain refinement have significantly enhanced the mechanical properties. Wang et al. [22] have shown that the nanostructured surfaces, produced by sandblasting, improved the corrosion resistance of AISI 304. Wang et al. [23] have also shown that nanocrystallized surfaces induced by shot peening could enhance the corrosion resistance of 1Cr18Ni9Ti stainless steel in 3.5% NaCl solution. In fact, the fraction of grain boundaries in the nanostructured surface obtained by shot peening may increase the atomic diffusivity of passivating elements to form a protective passive layer [23,24]. On the other hand, the mechanical properties such as fatigue, hardness, wear resistance and yield strength of nanocrystallized surface materials were effectively improved by severe shot peening [25–27]. However, the combined effect of wear and corrosion (tribocorrosion behavior) on nanocrystallized surface metals obtained by severe shot peening remains mostly unstudied.

The aim of this work is to improve the tribocorrosion properties of AISI 304L using severe shot peening (NanoPeening®) [28,29]. EBSD was used to determine the microstructure of the nanopeened layer. Tribocorrosion studies were performed in olive pomace/tap water filtrate with pin-on-disc tribometer. Tribocorrosion wear was qualitatively studied to characterize the wear track. Quantitative analysis was carried out to determinate material loss.

2. Material and methods

2.1. Treatment

AISI 304L grade was used to prepare samples of 10 mm of height and 25 mm of diameter. The chemical composition of AISI 304L was given in Table 1. Samples were mechanically polished using sandpaper from grade 120 to 1200 to prepare them for nano-scale surface peening. Nano-scale surface peening was realized by Winoa company (NanoPeening® treatment) [30–32]. The treatment objective is to transform the surface of metals by reducing grain size down to a “nanometric” scale only by a mechanical operation based on Blasting Shot Peening [30]. In fact, it consists on the projection of shots by a very careful selection of the operating conditions [31]. The main parameters were: the shot diameters, the projected speed, the incidence angle and the recovery rate are ranged between 0.1 and 2 mm, 40 and 100 m s^{-1}, 10 and 45°, 1000 and 2000%, respectively. The processing duration is about few minutes [30–32].

2.2. Tribocorrosion tests

To investigate the effect of treatment on the tribocorrosion behavior of AISI 304L, the coupling of electrochemical methods with tribological tests was conducted. In fact, an electrochemical cell was mounted on a pin-on-disc tribometer. The cell was filled with electrolyte (pomace olive/tap water filtrate). It was prepared from the olive pomace collected from olive oil press and mixed with tap water. The obtained paste was filtrated to extract the test solution. The average pH value of the prepared electrolyte was about 5. The amount of chloride and sulfate in the filtrate was 0.027 and 0.012 mol/l, respectively. For the corrosion tests, a three electrode cell was used with a Solartron (1286) potentiostat and Solartron (1250) Frequency Reponse Analyser. The working electrode was a nanopeened AISI 304L sample, coated with resin to obtain a working area of 4.52 cm^2 (A_0). An Ag/Ag-Cl/KCl saturated electrode was used as a reference electrode which was characterized by $E_{Ag\text{-}AgCl}$ = + 0.200 V/Standard Hydrogen Electrode (SHE). The counter electrode was a platinum one. For tribological tests, an alumina pin with a spherical tip of 100 mm as radius was chosen to be the counter body. Sliding tests were performed at a normal force and rotation speed of respectively 5 N and 0.0628 m/s. According to the Hertz elastic theory, the normal force leads to maximum contact pressure of 82 MPa and a contact radius of 0.14 mm. The wear track diameter is 10 mm.

The tribocorrosion protocol test entailed three phases: stabilization before sliding test (stage 1), sliding test (stage 2), and final stabilization after sliding test (stage 3), as shown in Fig. 1. Cyclic potentiodynamic polarization curves were performed before sliding for a scan rate of 0.5 mV s^{-1} after three hours of immersion in the electrolyte. Free corrosion potential as a time function (OCP) and electrochemical impedance measurements (EIS) were performed during stage 1 and 2. EIS

Table 1
Normalized chemical composition of AISI 304L [33].

Elements	C	Si	Mn	P	S	Cr	Ni
Chemical composition [wt%]	≤ 0.02	≤ 1	≤ 2	≤ 0.04	≤ 0.03	17–18	9–11

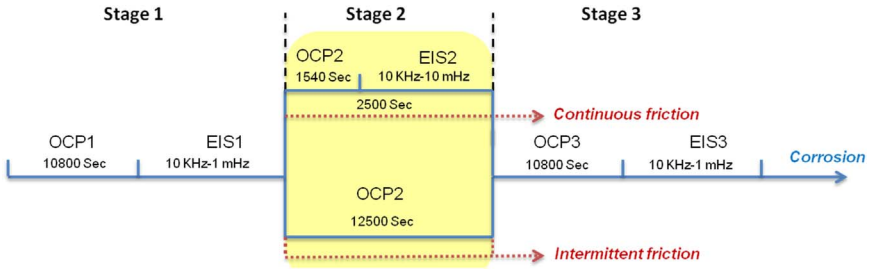

Fig. 1. Schematic representation of the tribocorrosion protocol.

was performed with a potential frequency which ranges between 1 mHz and 10 kHz during stage 1, and between 10 mHz and 10 kHz during stage 2. The amplitude of the sinusoidal voltage signal was 20 mV.

Two sliding types were carried out, continuous and intermittent ones. Continuous sliding was characterized by a permanent rotation of the pin during the whole test. However, intermittent sliding test consisted in the pin rotation for one period of time t_r = 0.5 s, and pin stop for another given period of time, t_{stop} = 2 s. The latency time of one cycle, t_{lat}, is the sum or t_r and t_{stop} [4,28,29].

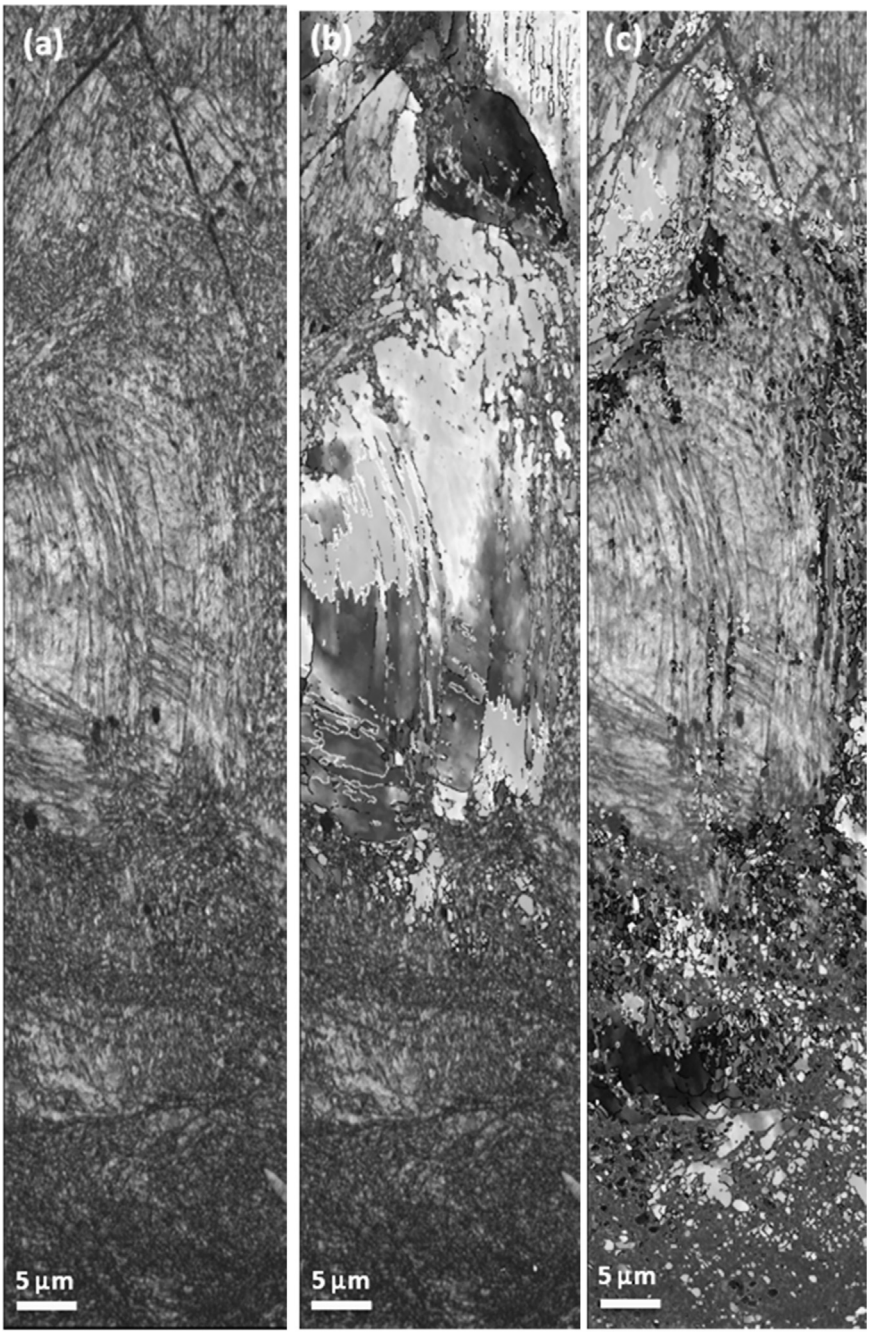

Fig. 2. EBSD map acquired in the intermediate layer (between 60 and 150 µm from the surface): (a) Kikuchi Pattern Quality map, (b) austenite IPF//Z map and (c) ferrite IPF//Z map.

2.3. Samples characterization

After nano-scale surface peening, samples were polished using sandpaper from grade 400 until 1200 to get a final roughness (Ra) of about 0.11 µm which is suitable for tribocorrosion test. The cross section surface was also polished with several grades of alumina pastes down to 1 µm to obtain a mirror surface Ra = 0.08 µm) in order to characterize the microstructure by EBSD. The JEOL JSM-6500F SEM equipped with AZTEC EBSD system from Oxford Instruments was used in this work. These experiments were carried out with an acceleration voltage of 20 kV and a working distance of 15 mm.

During sliding, the coefficient of friction (COF) was measured and wear was quantified using profilometric measurements (station Micromeasure STIL, France) in four areas regularly spaced along the sliding track. The wear track volume was determined by multiplying the area of the profiles by the wear track perimeter. Optical microscope and a scanning electron microscope (JEOL, JSM-T220A model) were used to analyze wear tracks.

3. Results and discussion

3.1. Microstructure analyses

Microstructural analyses was performed on cross sections of nanopeened AISI 304L using EBSD. EBSD and SEM analysis confirmed that the nano-scale surface peening produced a nanosized microstructure over a depth of 150 µm from the top surface. Three different regions can be clearly identified in the treated surface. The first zone corresponds to the bulk material. Its microstructure remained close to the as-received material and consists in an equiaxe grains having a means size of approximately 23 µm. The second layer extended from 60 to 150 µm below the surface. The microstructure consisted in deformed prior austenite grains, partially transformed to α' martensite due to severe plastic deformation, as revealed by the EBSD map Fig. 2 [34,35]. In fact, austenite was deformed by twining to get α' matensite which preferentially nucleates at the intersection of the deformation twins. Similar results have also been noted in AISI type 304 stainless steels in the literature [36,37].

The IPF color code is given in Fig. 2 (notice that the indexing rate was only of 60%).

The third layer consisted in grains of several tens of nanometers as seen on the Back Scattered Electron (BSE) micrograph Fig. 3(a). This layer extended over 60 µm from the top surface. Inside the layer, larger ferrite grains were locally observed. When moving to the top layer, the transformation rate increased and the martensitic domains were progressively fragmented to nanosized ferrite grains building the top layer. Further EBSD showed that those nanosized grains were ferrite grains with a random texture as shown in Fig. 3(b). A mechanism of grain refinement was induced by severe plastic deformation [38,39]. Firstly, nano-scale surface peening process induces repeated high energy impacts at high rates onto the specimen surface. Then, dislocations are created and their number is increased due to the repeated impacts. Finally dislocations will be annihilated or rearranged to form small angle grain boundaries separating individual crystals, as proposed by Fecht [40].

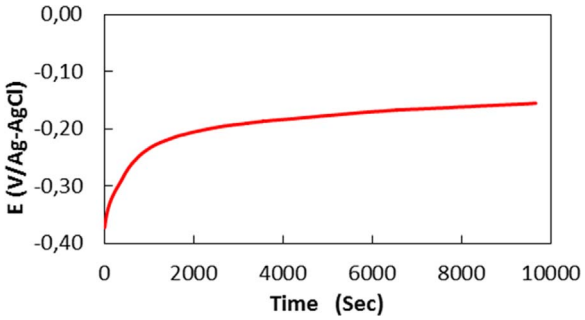

Fig. 4. Evolution of open circuit potential of nanopeened AISI 304L immersed in filtrate at 25 °C, without mechanical loading.

3.2. Corrosion tests without mechanical loading

The evolution of open circuit potential (OCP) versus time of the AISI 304L after nano-scale surface peening is shown in Fig. 4. It is clearly shown that free potential shifted to high value with increasing time and stabilized at OCP (E_{corr}) of about − 0.15 V/Ag-AgCl which indicates the formation of natural passive film. Also, the corrosion behavior of the passive layer was determined by cyclic polarization tests. The polarization curve of nanopeened AISI 304L, immersed in olive pomace/tap water filtrate, is presented in Fig. 5. The polarization curve reveals an active–passive transition between − 0.46 and − 0.26 V/Ag-AgCl. It was noted that the active peak is small due to the high ohmic drop. This phenomenon could be explained by the large distance separating the

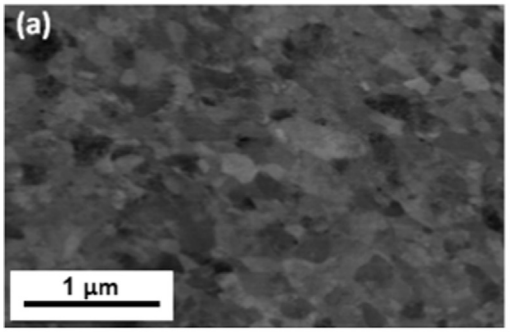

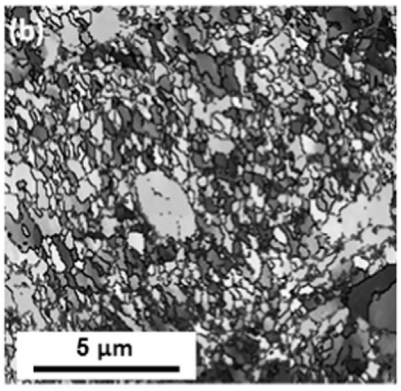

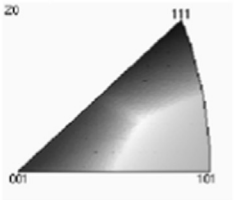

Fig. 3. Nanosized ferrite grains at the top layer of the nanopeened 304L sample (a) BSE micrograph close to the top surface, (b) Inverse Pole Figure (IPF) EBSD map of the ferrite phase - the map was acquired in the middle of the 60 µm thick top layer.

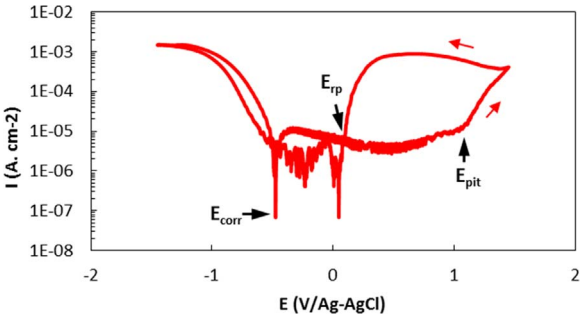

Fig. 5. Cyclic polarization curve of nanopeened AISI 304L immersed in filtrate at 25 °C. E_{corr}: Corrosion potential, E_{prot}: Protection potential, E_{pit}: pitting potential.

sample from reference electrode and the current magnitude. The curve displays a large passive region that extends to ~ 1.4 V and which is characterized by a passive current density of about 7.5×10^{-6} A/cm^2.

After the establishment of the passive range, the pitting corrosion of treated sample starts at a breakdown potential of 1.2 V/Ag-AgCl. By reversing the scan towards lower potentials, a positive hysteresis is observed in the cyclic polarization curves, indicating that in the potential range (0.4–1.5 V/Ag-AgCl) a metal dissolution occurs at the sample surfaces by pitting [41]. The repassivation power, which means the ability to reform the passive film, is measured by the protection potential (E_{prot}) which reaches 0.05 V/Ag-AgCl. It is clearly seen that E_{corr} is lower than E_{prot} which indicates that the repassivation ability is greater. In fact the surface sample at open circuit potential is covered by adhesive, dense and stable oxide layer which acts as a barrier layer between metal and environment to protect the underlying substrate from high corrosion rates [42–44]. The passive film properties were also tested using electrochemical impedance spectra (EIS) on Nyquist and bode plots shown in Fig. 6. Fitting was performed with ZView2 software and equivalent electric circuit (EC) in Fig. 7 was proposed to model the experimental data.

The EC is composed by the solution resistance (R_s), the double layer capacitance (Cdl) and the polarization resistance (R_p). The polarization resistance R_p is directly related to the size of the circle Nyquist arc. The high Rp value of about 1.54×10^6 Ω indicates that nanopeened AISI 304L is covered with a dense Cr_2O_3 film in contact with the solution [22]. However the absolute value is constant at high frequencies giving the value of solution resistance which is about 48 Ω.

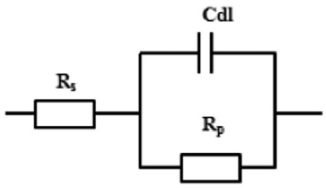

Fig. 7. Equivalent electric circuit.

3.3. Tribocorrosion tests

3.3.1. Corrosion tests under sliding

In order to determine the surface state and corrosion resistance of sample under sliding in filtrate, EIS were established at mean OCP of − 0.42 V/Ag-AgCl as shown in Fig. 8. The electrical equivalent circuit describing the surface in active state is presented in Fig. 7.

By simulating the experimental data with this equivalent circuit, the polarization resistance values (R_p) for treated sample is about 409.6 Ω cm^2 which indicates an active surface sample [29]. R_s = 45 Ω is the electrolyte resistance, and CPE is the capacitive element depending on frequency.

However, under intermittent sliding the OCP drop to more cathodic potential compared to continuous sliding. In fact, the wear track was repassivated after the stop time due to the short repassivation time about 200 ms [45]. Hence, a small reactive area of the nanopeened AISI 304L was exposed to the environment resulting in more cathodic potential. Moreover, the potential evolution of the treated metal versus time is slowly stabilized. EIS measurements can not be performed during such intermittent sliding tests because of the non stationery OCP during one cycle as shown in Fig. 9.

3.3.2. Friction and wear analyses

3.3.2.1. The effect of latency time. The COF was measured under both continuous and intermittent sliding as shown in Fig. 10. It is clearly shown that the COF was not affected by latency time for a cycle number below 1000. However, above 1000 cycles, the COF was decreased under intermittent sliding. This result could be explained by the effect of repassivation during stop time. In fact, the oxide debris act as a solid lubricant decreasing the contact forces [46]. After 3000 cycle, wear debris were ejected from the wear track. Therefore, friction coefficient is not affected by latency time.

In fact, under continuous sliding, the profile section of wear track, for treated samples, was characterized by the emergence of wedges suggesting a predominantly plastic flow regime (Fig. 11(a)). Therefore, adhesion mechanism could be emphasized. The existence of some grooves, observed in SEM images (Fig. 12(a)), proves that an abrasive

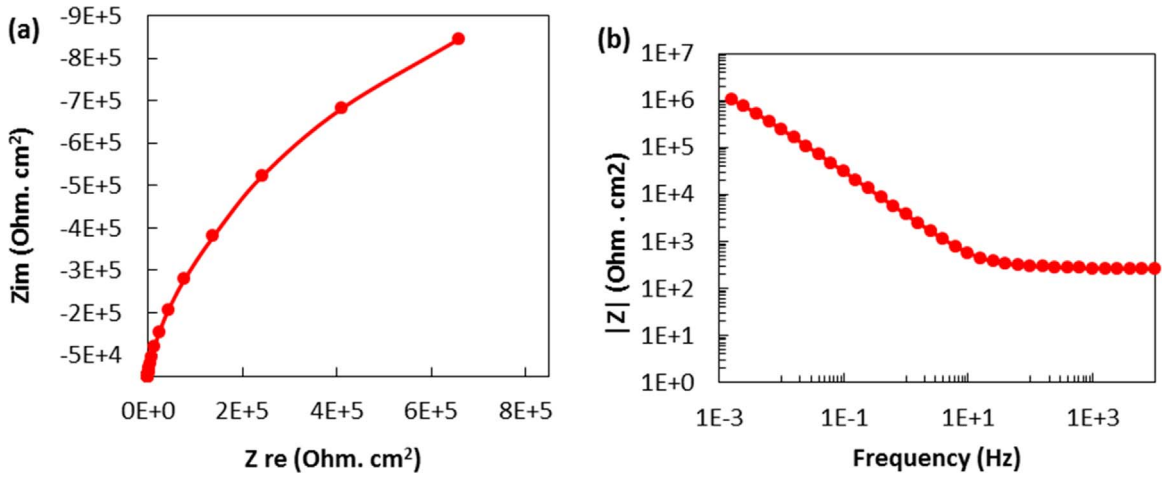

Fig. 6. Electrochemical impedance spectra: (a) Nyquist plot and (b) Bode plot of nanopeened AISI 304L immersed in filtrate at 25 °C, without mechanical loading.

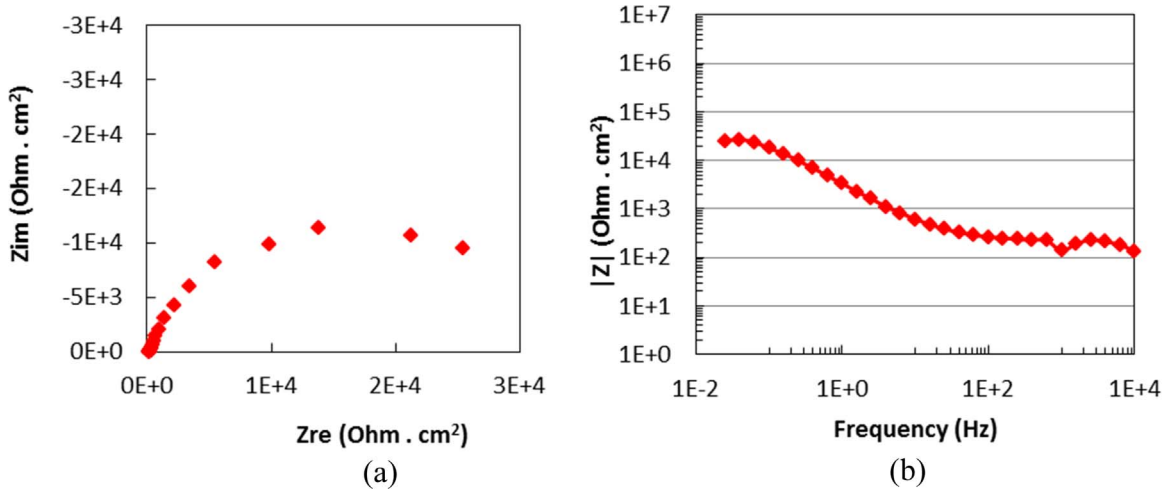

Fig. 8. Electrochemical impedance spectra: (a) Bode and (b) Nyquist plots at the mean open-circuit potential value under continuous sliding performed at 5 N and 0.0628 m/s on nanopeened AISI 304L immersed in filtrate at 25 °C.

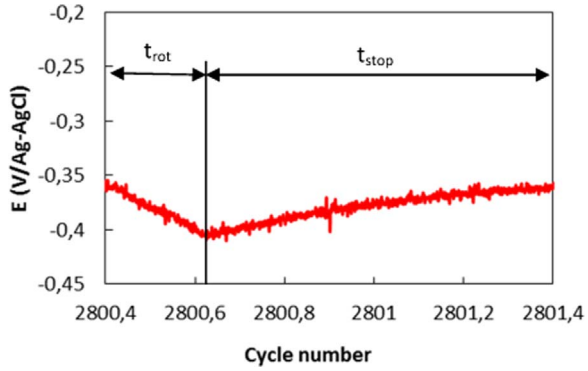

Fig. 9. Evolution of open circuit potential during one cycle under intermittent sliding performed at 5 N and 0.0628 m/s on nanopeened AISI 304L immersed in filtrate at 25 °C.

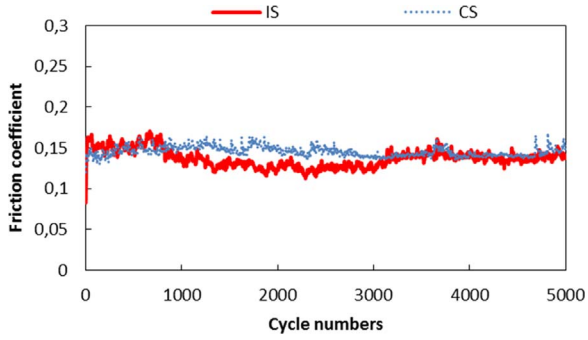

Fig. 10. Friction coefficient as a function of cycle numbers of nanopeened AISI 304L/alumina ball contacts under continuous (CS) and intermittent (IS) sliding.

mechanism could also exist. Indeed, sample surface was scratched by abrasive wear debris which were ejected, oxidized and accumulated around the wear track.

Whilst continuous sliding occurs on active surface state, intermittent sliding consists on a transition of wear behavior accompanied by a change of the wear track state. In fact, during each cycle, the wear track alternates between active and repassivated states. Obviously, the passive oxide layer which was created during t_{stop} will be destroyed during t_{rot}. Consequently, corrosive wear debris were ejected and caused then the appearance of deep abrasive scratches (Fig. 12(b)). Therefore, it is important to note that the main wear mechanism could be an abrasive one.

3.3.2.2. The effect of nano-scale surface peening. To determinate the effect of nano-scale surface peening, current results will be compared with our previous work [5]. The COF of the treated sample is lower than untreated one under continuous or intermittent sliding. The nanosized ferrite grains formed in the nanocrystallized passive layer are beneficial in reducing friction. Moreover, SEM observations show that the wear track produced on the treated sample has a similar morphology to that observed on untreated one, which reveals an abrasive mechanism. Fig. 13(a) and (b) and Table 2 compare the corrosion and mechanical contributions for both untreated and treated samples, respectively, under continuous and intermittent sliding.

The total wear loss after sliding in filtrate could be calculated according to a typical tribocorrosion protocol [4,28,29]. N. Diomidis et al. described the total wear loss in the wear track, W_{tr}, as the sum of four components according to Eq. (1)

$$W_{tr} = W^{c}_{act} + W^{c}_{repass} + W^{m}_{act} + W^{m}_{repass} \quad (1)$$

where W^{c}_{act} is material loss due to corrosion of active material in the wear track, W^{c}_{repass} is the material loss due to corrosion of repassivated material in the wear track, W^{m}_{act} is material loss due to mechanical wear of the active material in the wear track and W^{m}_{repass} is the material loss due to the mechanical wear of repassivated material in the wear track.

As compared to the untreated sample, the nanopeened sample experiences a significant decrease in total wear loss, with a predominant mechanical wear contribution. Under continuous sliding, the W^{m}_{act} decreases by 20% compared to untreated sample but the W^{c}_{act} remains unchanged with treatment, which explains the increase of the ratio K_c presented in Table 2.

Under intermittent sliding, all wear contributions, W^{c}_{act}, W^{m}_{act}, W^{c}_{repass} and W^{m}_{repass}, of treated sample are lower than that of untreated one. This fact indicates an improvement of the mechanical and corrosion resistances. Therefore, the mechanical resistance seems to be the most improved because K_c ratio rises with treatment (Table 2). In addition, the increase of K_m ratio shows that the improvement of mechanical removal resistance is essentially due to the existence of nanocrystallized passive layer which provides more protection to the material against corrosion and especially mechanical wear [28]. Improvement in corrosion resistance resulted from the Cr enrichment of surface layer due to faster diffusion of Cr through grain boundaries [47]. Ferritizers such as Cr and Mo were significantly enriched in ferrite, while austenitizers such as Ni and nitrogen were enriched in austenite [48]. The higher content of chromium in ferrite is suspected to have produced a stronger and thicker chromium oxide protection on nanopeened AISI 304L. Besides, the mechanical wear decrease could be attributed to the hardness increase as a result of nano-scale surface

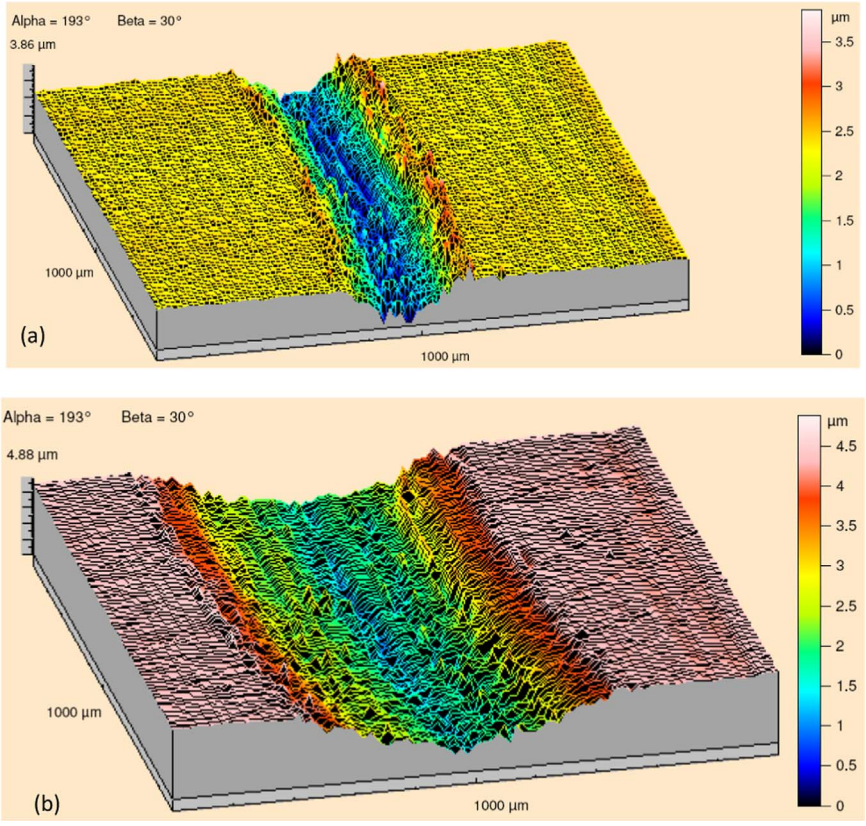

Fig. 11. 3D dimensional image of the wear track determined by optical profilometry on AISI nanopeened 304L: (a) treated under continuous and (b) treated intermittent sliding.

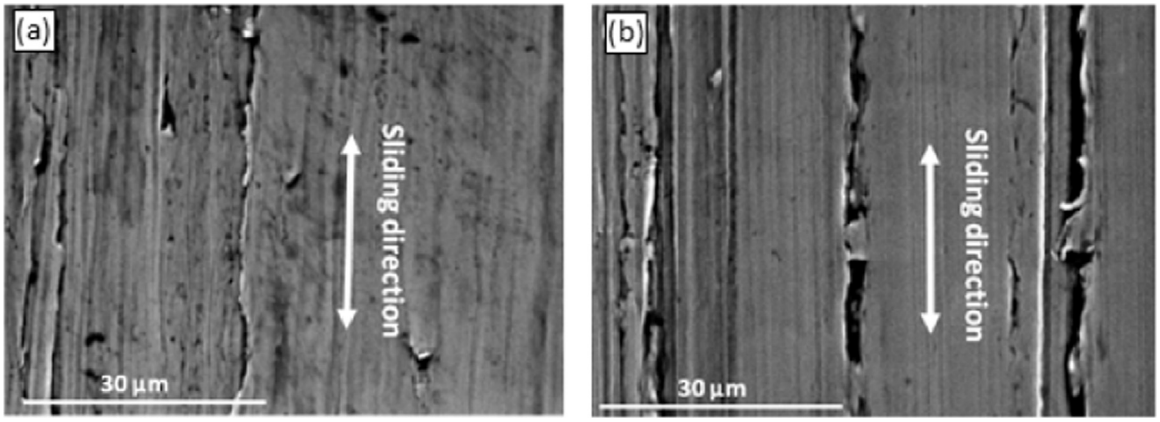

Fig. 12. Scanning electron microscope observations of the wear track on nanopeened AISI 304L: (a) under continuous and (b) intermittent sliding.

Table 2
Tribocorrosion components and k_c and $_{Km}$ ratio obtained on nanopeened AISI 304L under intermittent sliding.

304L	W^c_{act} (cm^3/cycle)	W^m_{act}	W^c_{repass}	W^m_{repass}	A_{act} (cm^2)	A_{repass}	k_c	k_m
Continuous sliding								
Untreated	5.9×10^{-11}	1.7×10^{-09}	–	–	0.057	–	3×10^{-02}	–
Treated	6.2×10^{-11}	1.5×10^{-09}	–	–	0.036	–	4×10^{-02}	–
Intermittent sliding								
Untreated	3.7×10^{-10}	6.9×10^{-09}	2.7×10^{-16}	1.2×10^{-09}	0.222	1.5×10^{-04}	4.6×10^{-02}	4×10^{-03}
Treated	2.3×10^{-10}	3.8×10^{-09}	9.0×10^{-17}	8.1×10^{-10}	0.092	6.1×10^{-05}	5.2×10^{-02}	3×10^{-03}

peening. The hardness increase is due to grain refinement in the surface layer [49]. It can be concluded that the nanosized ferrite grains are helpful to the surface strengthening of materials. In fact, the higher hardness subsurface and nanocrystallized microstructure have a tendency to decrease the wear resistance [49,50]. The effect of the mechanical action is revealed by the distribution of microhardness in the wear track as shown in Fig. 14.

In the case of untreated sample, it was clearly noted that measured microhardness inside the wear track was higher than outside the track. Thus, it could be attributed to the severe work hardening by the sliding action of the alumina pin. Also, it seems that grooved and scratched surfaces were harder than the non-grooved surfaces. So, the hardness of the sheared material at the base of the scratch was in the range of 400 $HV_{0.05}$ which corresponds to a heavily work-hardened metal. However, in the case of treated samples, the microhardness measurements were not affected by the sliding action. This indicates that the nanocrystallized layer is work-hardened enough by the nano-scale surface

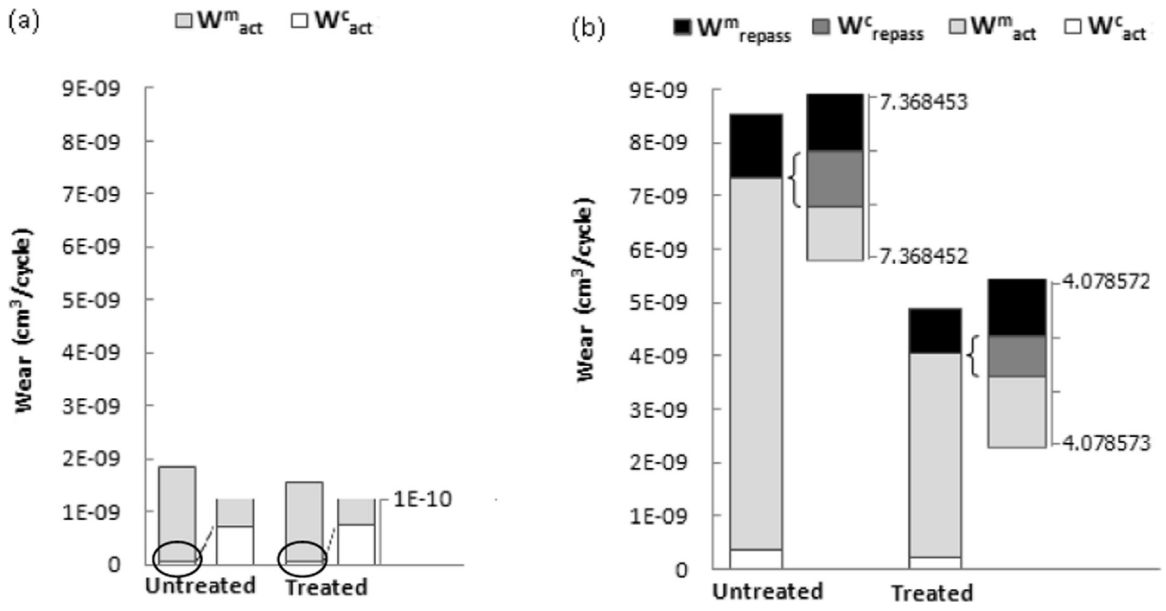

Fig. 13. Contribution of wears obtained on nanopeened AISI 304L under (a) continuous ($t_{lat}(cs)$ = 0.5 s) and (b) intermittent ($t_{lat(is)}$ = 2.5 s) sliding against alumina pin (5 N, 0.0628 m/s) in filtrate olive pit/tap water.

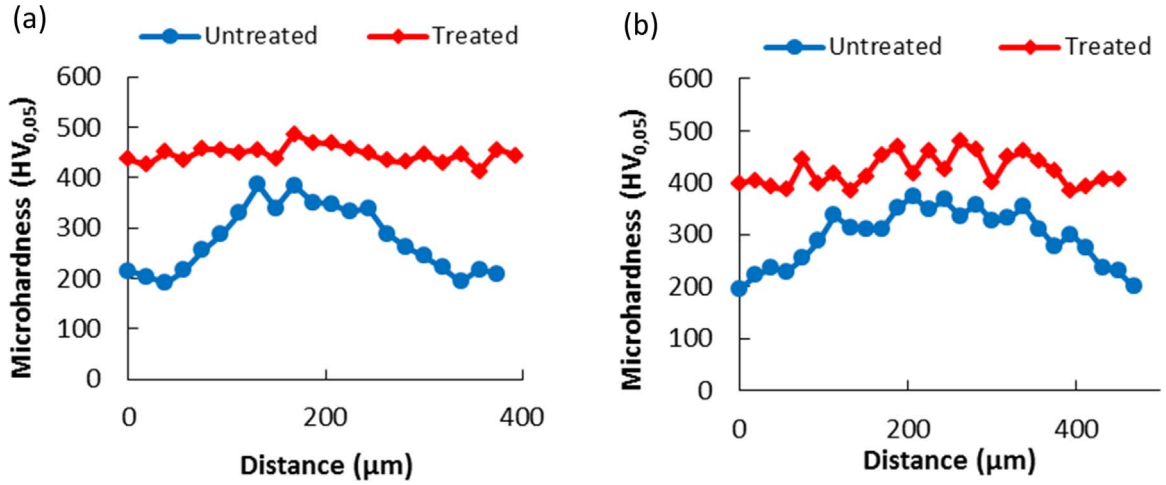

Fig. 14. Microhardness profile in the wear track width under (a) continuous and (b) intermittent sliding.

peening until reaching saturation which matches up to higher microhardness values. The severe shot peening treatment forms refined ferrite domains and enhances microhardness, preventing the pin and the particles from penetration to non-nanocrystallized zone. As a result, the wear track depth decreases as shown in Fig. 13 and the wear resistance is well enhanced especially for intermittent sliding as presented in Fig. 14.

4. Conclusions

The objective of this work was to study the effect of nano-scale surface peening on the tribocorrosion behavior of AISI 304L rubbed against alumina pin under continuous and intermittent sliding in olive pomace/tap water filtrate.

(a) EBSD allows the detection of the microstructural changes caused by the deformation twinning, the development of martensitic and ferritic transformations accruing during treatment. The top layer, of 150 µm thickness, consisted in ferrite grains of several tens of nanometer.
(b) Under both continuous and intermittent sliding, wear mechanism was dominated by abrasion. For the continuous sliding, an adhesion mechanism could also be present.
(c) Under continuous sliding, the corrosion resistance was not changed with treatment. However, mechanical resistance was well improved. Two factors contributed to such an enhancement in mechanical wear resistance that are the nanocrystallized layer structure and the high hardness occurred by the treatment.
(d) Under intermittent sliding, the nano-scale surface peening improves corrosion and mechanical resistance. The nanocrystallized top layer consists on ferrite grains which are enriched with Cr and Mo contents. The improved corrosion resistance could be explained by the Cr diffusion on the protective film. The mechanical wear resistance was improved due to the work-hardened surface obtained after the nano-scale surface peening.

Acknowledgments

This research was partially financed by the European Project EU-FP7 grant Oil & Sugar (295202). Also, the present authors thank Winoa company which kindly provided nano-peened samples.

References

[1] F. Ben Saada, K. Elleuch, Damage of stainless steel components by olive paste, Tribol. Trans. (2015), http://dx.doi.org/10.1080/10402004.2015.1115569.

[2] T. Wang, J. Yu, B. Dong, Surface nanocrystallization induced by shot peening and its effect on corrosion resistance of 1Cr18Ni9Ti stainless steel, Surf. Coat. Technol. 200 (2006) 4777–4781.

[3] K. Lu, J. Lub, Nanostructured surface layer on metallic materials induced by surface mechanical attrition treatment, Mater. Sci. Eng. A 375 (2004) 38–45.

[4] F. Ben Saada, Z. Antar, K. Elleuch, P. Ponthiaux, On the tribocorrosion behavior of 304L stainless steel in olive pomace/tap water filtrate, Wear 328–329 (2015) 509–517.

[5] J. Perret, E. Boehm-Courjault, M. Cantoni, S. Mischler, A. Beaudouin, W. Chittyd, J.-P. Vernot, EBSD, SEM and FIB characterisation of subsurface deformation during tribocorrosion of stainless steel in sulphuric acid, Wear 269 (2010) 383–393.

[6] Bing Liu, Xian Zhang, Gui-yong Xiao, Yu-peng Lu, Phosphate chemical conversion coatings on metallic substrates for biomedical application: a review. ⟨http://doi.org/10.1016/j.msec.2014.11.038⟩.

[7] S. Zhang, C.L. Wu, C.H. Zhang, M. Guan, J.Z. Tan, Laser surface alloying of FeCoCrAlNi high-entropy alloy on 304 stainless steel to enhance corrosion and cavitation erosion resistance, Opt. Laser Technol. 84 (2016) 23–31.

[8] W.J. Yang, M. Zhang, Y.H. Zhao, M.L. Shen, H. Lei, L. Xu, J.Q. Xiao, J. Gong, B.H. Yu, C. Sun, Enhancement of mechanical property and corrosion resistance of 316 L stainless steels by low temperature arc plasma nitriding, Surf. Coat. Technol. 298 (2016) 64–72.

[9] W. Yanfang, L. Qinglong, X. Lijun, S. Zhiqiang, Laser cladding Fe-Cr-Si-P amorphous coatings on 304L stainless, Rare Met. Mater. Eng. 43 (2) (2014) 0274–0277.

[10] A. Bahri, E. Kaçar, S.S. Akkaya, K. Elleuch, M. Ürgen, Wear protection potential of TiN coatings for 304 stainless steels used in rotating parts during olive oil extraction, J. Surf. Coat. ⟨http://doi.org/10.1016/j.surfcoat.2016.07.067⟩.

[11] F. Maury, F.-D. Duminica, TiOxNy coatings grown by atmospheric pressure metal organic chemical vapor deposition, Surf. Coat. Technol. 205 (2010) 1287–1293.

[12] B. Mahmoudi, M.J. Torkamany, A.R. Sabour Rouh Aghdam, J. Sabbaghzade, Laser surface hardening of AISI 420 stainless steel treated by pulsed Nd:YAG laser, Mater. Des. 31 (2010) 2553–2560.

[13] W. Pacquentin, N. Caron, R. Oltra, Effect of microstructure and chemical composition on localized corrosion resistance of a AISI 304L stainless steel after nano-pulsed-laser surface melting, Appl. Surf. Sci. 356 (2015) 561–573.

[14] T. Balusamy, T.S.N. Sankara Narayanan, K. Ravichandran, Il Song Park, Min Ho Lee, Influence of surface mechanical attrition treatment (SMAT) on the corrosion behaviour of AISI 304 stainless steel, Corros. Sci 74 (2013) 332–344.

[15] X.J. Cao, Y.S. Pyoun, R. Murakami, Fatigue properties of a S45C steel subjected to ultrasonic nanocrystal surface modification, Appl. Surf. Sci. 256 (2010) 6297–6303.

[16] C.M. Suh, G.H. Song, M.S. Suh, Y.S. Pyoun, Fatigue and mechanical characteristics of nano-structured tool steel by ultrasonic cold forging technology, Mater. Sci. Eng.: A 443 (2007) 101–106.

[17] S. Bagherifard, M. Guagliano, Fatigue behavior of a low-alloy steel with nanostructured surface obtained by severe shot peening, Eng. Fract. Mech. 81 (2012) 56–68.

[18] S. Bagherifard, M. Guagliano, Influence of mesh parameters on FE simulation of severe shot peening (SSP) aimed at generating nanocrystallized surface layer, Procedia Eng. 10 (2011) 2923–2930.

[19] Z. Ni, X. Wang, J. Wang, Erdong Wu, Characterization of the phase transformation in a nanostructured surface layer of 304 stainless steel induced by high-energy shot peening, Physica B 334 (2003) 211–228.

[20] Y. Todaka, M. Umemoto, K. Tsuchiya, Comparison of nanocrystalline surface layer in steels formed by air blast and ultrasonic shot peening, Mater. Trans. 45 (2004) 376–379.

[21] P. Tadge, P. Kumar Gupta, C. Sasikumar, Surface nano-crystallization of AISI 304 stainless steel through shot peening technique, Mater. Today: Proc. 2 (2015) 3245–3250.

[22] X.Y. Wang, D.Y. Li, Mechanical and electrochemical behavior of nanocrystalline surface of 304 stainless steel, Electrochim. Acta. 47 (2002) 3939–3947.

[23] X.Y. Wang, D.Y. Li, Mechanical, electrochemical and tribological properties of nano-crystalline surface of 304 stainless steel, Wear 255 (2003) 836–845.

[24] C. Zhong, L. Liu, Y. Wu, Y. Deng, B. Shen, B. Shu, W. Hu, Diffusion behavior of aluminum in the surface layer of iron processed by shot peening, Mater. Lett. 64 (2010) 1407–1409.

[25] G. Liu, S.C. Wang, X.F. Lou, J. Lu, K. Lu, Low carbon steel with nanostructured surface layer induced by high-energy shot peening, Scr. Mater. 44 (2001) 1791–1795.

[26] H. Li-feng, W. Ying-hui, L. Bao-sheng, X. Bing-she, Microstructure evolution of AZ91D induced by high energy shot peening, Trans. Nonferr. Met. Soc. China 18 (2008) 1053–1057.

[27] W. Yan, L. Fang, Z. Zheng, K. Sun, Y. Xu, Effect of surface nanocrystallization on abrasive wear properties in Hadfieldsteel, Tribol. Int. 42 (2009) 634–641.

[28] N. Diomidis, J.P. Celis, P. Ponthiaux, F. Wenger, Tribocorrosion of stainless steel in sulfuric acid: Identification of corrosion–wear components and effect of contact area, Wear 269 (2010) 93–103.

[29] N. Diomidis, J.P. Celis, P. Ponthiaux, F. Wenger, A methodology for the assessment of the tribocorrosion of passivating: metallic materials, Lubr. Sci. 21 (2009) 53–67.

[30] T. Prezeau, T. Muller, M. Baron, J. Samuel, E. Dransar, Surface Treatment of A Metal Part, Patented no. EP 2721190 A1.

[31] T. Prezeau, T. Muler, E. Dransar, Y. Giraud, Amélioration par un prétraitement mécanique de NanoPeening® des performances des traitements thermochimiques, Traitements Mat. (2011) 37–43.

[32] C. Morel, M. Guagliano, Surface nanostructuring through a technique derived from shot-peening: recent advances, The Shot Peening | Blast Cleaning Library. ⟨http://www.shotpeener.com/library/pdf/2014001.pdf⟩.

[33] A. Van Herpen, B. Reynier, C. Phalippou, Effect of test duration on impact/sliding wear damage of 304L stainless steel at room temperature: metallurgical and micromechanical investigations, Wear 249 (2001) 37–49.

[34] Z. Ni, X. Wang, J. Wang, E. Wu, Characterization of the phase transformation in a nanostructured surface layer of 304 stainless steel induced by high-energy shot peening, Physica B 334 (2003) 221–228.

[35] C. Ye, A. Telang, A.S. Gill, S. Suslov, Y. Idell, K. Zweiacker, J.M.K. Wiezorek, Z. Zhou, D. Qian, S. Ramaiah Mannava, V.K. Vasudevan, Gradient nanostructure and residual stresses induced by Ultrasonic Nano-crystal Surface Modification in 304 austenitic stainless steel for high strength and high ductility, Mater. Sci. Eng. A 613 (2014) 274–288.

[36] S.J. Lee, Y.M. Park, Y.K. Lee, Reverse transformation mechanism of martensiteto austeniten a metastable austenitic alloy, Mater. Sci. Eng. A 515 (2009) 32–37.

[37] R. Wanga, Z. Zhengb, Q. Zhoua, Y. Gaoa, Effect of surface nanocrystallization on the sensitization anddesensitization behavior of Super 304H stainless steel, Corros. Sci 111 (2016) 728–741.

[38] M. Sato, N. Tsuji, Y. Minamino, Y. Koizumi, Formation of nanocrystalline surface layers in various metallic materials by near surface severe plastic deformation, Sci. Technol. Adv. Mater. 5 (2004) 145–152.

[39] S. Bagherifard, I. Fernandez-Pariente, R. Ghelichi, M. Guagliano, Effect of severe shot peening on microstructure and fatigue strength of cast iron, Int. J. Fatigue 65 (2014) 64–70.

[40] H.J. Fecht, G.C. Hadjipanayis, R.W. Siegel (Eds.), Nanophase Materials, Kluwer Academic Publishers, Dordrecht (The Netherlands), 1994.

[41] R.A. Silva, M.A. Barbousa, Electrochemical behaviour of laser treated AISI 316L Stainless stell surfaces in physiological solution, Clin. Mater. 7 (1991) 31–27.

[42] K.E. Heusler, Fundamental aspects of the passivation of metals and semiconductors, Mater. Sci. Forum 9 (1995) 185–188.

[43] M.B. Ives, J.L. Luo, J. Rodda, Passivity of metals and semiconductors, in: Proceedings of the Electrochemical Society Pennington, NY, 2000, pp. 99-42.

[44] P. Marcus, V. Maurice, Passivation of Metals and Semiconductors, and Properties of Thin Oxide Layers, Elsevier, Amsterdam, 2006 ISBN: 0-444-52224-7.

[45] J. Jiang, M.M. Stack, A. Neville, Modelling the tribo-corrosion interaction in aqueous sliding conditions, Tribol. Int. 35 (2002) 669–679.

[46] D.A. Green, R. Lewis, J. Cripps, Friction and wear testing for a down-hole oil well centralizer, Wear 263 (2007) 57–64.

[47] R.K. Gupta, N. Birbilis, The influence of nanocrystalline structure and processing route on corrosion of stainless steel: a review, Corros. Sci. (2014) 1–15, http://dx.doi.org/10.1016/j.corsci.2014.11.041.

[48] K. Hashimoto, K. Asami, K. Teramoto, An x-ray photo-electron spectroscopic study on the role of molybdenum in increasing the corrosion resistance of ferritic stainless steels in HC1, Corros. Sci 19 (1979) 3–14.

[49] W. Yan, L. Fang, Z. Zheng, K. Sun, Y. Xu, Effect of surface nanocrystallization on abrasive wear properties in Hadfield steel, Tribol. Int. 42 (2009) 634–641.

[50] J.S.C. Tang, C.C. Koch, The Hall-Petch relationship in nanocrystalline iron produced by ball milling, Scr. Metall. Mater. 24 (1990) 1599–1604.